FINITE-ELEMENT MODEL FOR NAILED WOOD JOINTS UNDER REVERSED CYCLIC LOAD

By Ying H. Chui,[1] Chun Ni,[2] and Lei Jiang[3]

ABSTRACT: This paper presents a nonlinear finite-element model for predicting the load-slip response of a single-shear nailed wood joint under reversed cyclic loading. Of particular interest is the post-yielding region of the load-slip response at which the deformation of the nail is large. In the proposed theory, the nail is modeled using a finite beam element approximation that incorporates the effects of large deformation and hysteretic nature of the stress-strain behavior of the material. The embedment behavior of wood under the action of a nail is described through a hysteresis model developed by the writers. In addition the effects of shear deformation in the nail and friction between nail and wood are incorporated into the model. Results from material tests conducted to characterize the embedment behavior of wood and stress-strain curve of nail material, and from joint tests to verify the finite-element model, are presented. A comparison of test data with model predictions demonstrates the validity of the model. The present theory can be extended to analyze wood joints containing other dowel-type fasteners.

INTRODUCTION

The ability of a structure to absorb input loading energy through ductile deformations of its elements is a key factor in its performance under extreme environmental loading conditions such as those arising from earthquakes and hurricanes. In fact, for structures that contain brittle elements, the ability to deform in a ductile manner without significant strength degradation is not only desirable but essential in order to prevent collapse during these extreme loading conditions [Paulay and Priestley (1992)]. Timber structures are an example of such a system, since the material generally fails in a brittle manner. The main source of ductility in timber structures is therefore in the mechanically fastened joints, especially those with dowel-type fasteners such as nails and bolts. Mechanically fastened timber joints have traditionally been characterized under monotonic loading conditions. Recent concerns on the behavior of structures during earthquakes and hurricanes have led to the need to elucidate the behavior of timber joints under reversed cyclic loading conditions.

Research in the area of joint behavior under reversed cyclic loading has to date focused largely on the influence of various joint parameters on performance characteristics such as ductility, strength, shape of hysteresis loops, and strength degradation through ad hoc testing. These included single-fastener nailed [Soltis and Mtenga (1985); Dolan and Madsen (1992); Ni and Chui (1994)] and bolted [Gutshall et al. (1994); Daneff et al. (1996)] joints, and moment-resisting joints containing dowels [Ceccotti and Vignoli (1990)] or glulam rivets [Hattar and Cheng (1995)]. In general, it is concluded that only joints with small-diameter fasteners, such as nails, glulam rivets, and small-diameter dowels and bolts, are capable of failing in a ductile manner. Also, strength of joints increases with increasing loading frequency. However, increased loading frequency leads to more pronounced strength degradation, as do increased loading cycles. The load-deformation response of mechanically fastened timber joints generally exhibits some nonlinear hysteresis effects. Analytical modeling of the behavior of structural systems containing these joints calls for the appropriate modeling of this hysteresis behavior. Empirical modeling of joint response under reversed cyclic loading has also been investigated by a number of scientists [Kivell et al. (1981); Stewart (1987); Dolan (1989); Ceccotti and Vignoli (1990); Cecotti et al. (1994); Foliente (1994)].

In comparison with the testing efforts summarized above, attempts on analytical modeling of joint behavior under reversed cyclic loading have been scarce. Ni et al. (1993) and Cruz (1993) developed two simple analytical models for predicting the hysteretic response of nailed joints. The models are essentially similar except that Ni et al. (1993) considered the so-called mode III (plastic hinges in both members) whereas Cruz (1993) considered mode II (plastic hinge in the point side member). The theory was based on the integration of embedment loads developed in the joint members when loaded by a nail. Input properties are the load-embedment behavior of wood and nail bending properties. When determining properties of nailed joints that have significant influences on the behavior of structures under seismic loading, the post-yielding region is generally of great interest to engineers. In this region, the deformation of the nail is usually large, and therefore models based on small-deflection theory do not yield reliable predictions. Analysis techniques based on large-displacement theory are required. Such a model was developed by Prion and Foschi (1994) for dowelled wood joints using finite-element approximations. That model is an extension of an earlier monotonic beam-on-foundation model by Foschi (1974). The limitations of Prion and Foschi's model are that it ignores the effects of cyclic response of fastener material, shear deformation in the fastener, friction between fastener and wood, and the withdrawal effect of the fastener. These factors are considered important under reversed cyclic loads. The model presented here is a large-displacement finite-element model, which considers these factors. It predicts the response of a single-shear nailed joint to an arbitrary reversed cyclic loading function.

THEORY OF MODEL

In the proposed model a two-member nailed joint is represented by an assemblage of elements. To adequately account for the influential factors, three types of elements are required for the nail, wood, and frictional effects between nail and wood. The nail is represented by beam elements; the load-embedment characteristics of the wood beneath the nail, by spring elements; the friction between nail and wood, by link-

[1]Assoc. Prof., Facu. of Forestry and Envir. Mgmt., Univ. of New Brunswick, Fredericton, New Brunswick, Canada.

[2]Res. Engr., Facu. of Forestry and Envir. Mgmt., Univ. of New Brunswick, Fredericton, New Brunswick, Canada.

[3]Sr. Res. Engr., Martee Limited, Suite 400, 1888 Brunswick Street, Halifax, Nova Scotia, Canada.

Note. Associate Editor: Dan L. Wheat. Discussion open until June 1, 1998. To extend the closing date one month, a written request must be filed with the ASCE Manager of Journals. The manuscript for this paper was submitted for review and possible publication on March 10, 1997. This paper is part of the ***Journal of Structural Engineering***, Vol. 124, No. 1, January, 1998. ©ASCE, ISSN 0733-9445/98/0001-0096–0103/ $4.00 + $.50 per page. Paper No. 15286.

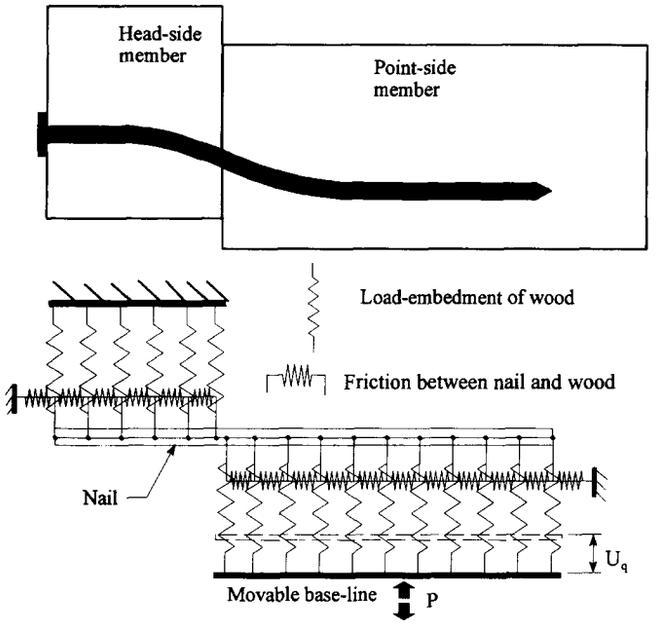

FIG. 1. Assemblage of Finite Element for Nailed Wood Joint

age elements. Fig. 1 shows the manner in which a single-shear nailed wood joint is modeled.

Since the problem is nonlinear, a solution is achieved by an iterative technique over time. Here time is used as a convenient variable that denotes different intensities of load applications and correspondingly different configurations. Solution at time step $t + \Delta t$ is obtained by considering the force equilibrium of the fastener and that of the embedment springs in the point-side member,

$$^{t+\Delta t}\begin{Bmatrix}\mathbf{R}\\ P\end{Bmatrix} = {}^{t+\Delta t}\begin{Bmatrix}\mathbf{F}\\ f\end{Bmatrix} \tag{1}$$

where $\mathbf{F}$ = vector of fastener internal forces; $\mathbf{R}$ = vector of externally applied nodal loads; P = total applied load; and f = total embedment force of point-side member.

Eq. (1) can be linearized to an incremental matrix form of the ith iteration at time $t + \Delta t$

$$\begin{bmatrix}\mathbf{K}_N + \mathbf{K}_{LM} + \mathbf{K}_{LF} + \mathbf{K}_{UM} + \mathbf{K}_{UF} & -\mathbf{K}_{LM}\mathbf{I}\\ -(\mathbf{K}_{LM}\mathbf{I})^T & \sum_{i=1}^{N_L}\mathbf{K}_{LM_i}\end{bmatrix}^{(i-1)}\begin{pmatrix}\mathbf{U}_N\\ U_q\end{pmatrix}^{(i)} = {}^{t+\Delta t}\begin{pmatrix}\mathbf{R}-\mathbf{F}\\ P-f\end{pmatrix}^{(i-1)} \tag{2}$$

where $\mathbf{K}_N$ = stiffness matrix of fastener; $\mathbf{K}_{LM}$ = embedment stiffness matrix of point-side member (diagonal); $\mathbf{K}_{LF}$ = friction stiffness matrix of point-side member (diagonal); $\mathbf{K}_{UM}$ = embedment stiffness matrix of head-side member (diagonal); $\mathbf{K}_{UF}$ = friction stiffness matrix of head-side member (diagonal); $\mathbf{I}$ = unit vector; N_L = number of nodes in point-side member; $\mathbf{U}_N$ = displacement vector of fastener; and U_q = movement of point-side member in the y-direction.

Fastener Deformation

A general three-node plane beam element (Fig. 2) is used to model the fastener, which takes into account large displacement, shear deformation, and material nonlinearity. The development of such element is based on the continuum mechanics approach. In this study, the total Lagrangian (TL) formulation is used. Using the principle of virtual work, the TL formulation can be expressed as [Bathe (1982)]

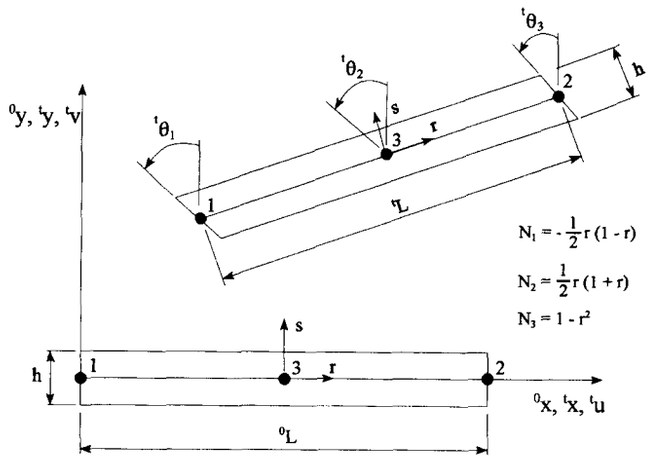

FIG. 2. Three-Node Beam Element Representing Nail

$$\int_{^0V} {}^{t+\Delta t}_{0}\mathbf{S}^T\delta({}^{t+\Delta t}_{0}\boldsymbol{\varepsilon})\,{}^0dV = {}^{t+\Delta t}\Pi \tag{3}$$

where ${}^{t+\Delta t}_{0}\mathbf{S}$ = second Piola-Kirchhoff stress vector corresponding to the configuration at time $t + \Delta t$ but measured in configuration at time 0; ${}^{t+\Delta t}_{0}\boldsymbol{\varepsilon}$ = Green-Lagrange strain vector in configuration at time $t + \Delta t$ referred to the configuration at time 0; and ${}^{t+\Delta t}\Pi$ = external virtual work in configuration at time $t + \Delta t$.

Because the configurations at time $t + \Delta t$ are unknown, in order to solve stresses ${}^{t+\Delta t}_{0}\mathbf{S}$ and strains ${}^{t+\Delta t}_{0}\boldsymbol{\varepsilon}$, the following incremental decomposition is used:

$${}^{t+\Delta t}_{0}\mathbf{S} = {}^{t}_{0}\mathbf{S} + {}_0\mathbf{S}; \quad {}^{t+\Delta t}_{0}\boldsymbol{\varepsilon} = {}^{t}_{0}\boldsymbol{\varepsilon} + {}_0\boldsymbol{\varepsilon} \tag{4a,b}$$

where ${}^{t}_{0}\mathbf{S}$ = second Piola-Kirchhoff stresses in configuration at time t referred to configuration at time 0; ${}^{t}_{0}\boldsymbol{\varepsilon}$ = Green-Lagrange strains in configuration at time t referred to configuration at time 0; ${}_0\mathbf{S}$ = incremental stresses from configuration at time t to configuration at time $t + \Delta t$ referred to configuration at time 0; and ${}_0\boldsymbol{\varepsilon}$ = incremental strains from configuration at time t to configuration at time $t + \Delta t$ referred to configuration at time 0.

For the plane beam element, the Green-Lagrange axial and shear strains at time t and $t + \Delta t$ referred to the configuration at time 0 are

$${}^{t}_{0}\varepsilon_x = \frac{\partial {}^tu}{\partial {}_0x} + \frac{1}{2}\left[\left(\frac{\partial {}^tu}{\partial {}_0x}\right)^2 + \left(\frac{\partial {}^tv}{\partial {}_0x}\right)^2\right] \tag{5a}$$

$${}^{t}_{0}\gamma_{xy} = \frac{\partial {}^tu}{\partial {}_0y} + \frac{\partial {}^tv}{\partial {}_0x} + \frac{\partial {}^tu}{\partial {}_0x}\frac{\partial {}^tu}{\partial {}_0y} + \frac{\partial {}^tv}{\partial {}_0x}\frac{\partial {}^tv}{\partial {}_0y} \tag{5b}$$

and

$${}^{t+\Delta t}_{0}\varepsilon_x = \frac{\partial {}^{t+\Delta t}u}{\partial {}_0x} + \frac{1}{2}\left[\left(\frac{\partial {}^{t+\Delta t}u}{\partial {}_0x}\right)^2 + \left(\frac{\partial {}^{t+\Delta t}v}{\partial {}_0x}\right)^2\right] \tag{6a}$$

$${}^{t+\Delta t}_{0}\gamma_{xy} = \frac{\partial {}^{t+\Delta t}u}{\partial {}_0y} + \frac{\partial {}^{t+\Delta t}v}{\partial {}_0x} + \frac{\partial {}^{t+\Delta t}u}{\partial {}_0x}\frac{\partial {}^{t+\Delta t}u}{\partial {}_0y} + \frac{\partial {}^{t+\Delta t}v}{\partial {}_0x}\frac{\partial {}^{t+\Delta t}v}{\partial {}_0y} \tag{6b}$$

where ${}^tu$ and ${}^tv$ denote the displacements in the global x- and y-directions, respectively, in the configuration at time t.

Subtracting (5) from (6), the incremental strains can be obtained as follows:

$${}_0\boldsymbol{\varepsilon} = {}_0\mathbf{e} + {}_0\boldsymbol{\eta} \tag{7}$$

where

$$ {}_0\mathbf{e} = \begin{pmatrix} {}_0\varepsilon_x \\ {}_0\gamma_{xy} \end{pmatrix} = \begin{pmatrix} \dfrac{\partial u}{\partial {}_0x} + \dfrac{\partial {}^t u}{\partial {}_0x}\dfrac{\partial u}{\partial {}_0x} + \dfrac{\partial {}^t v}{\partial {}_0x}\dfrac{\partial v}{\partial {}_0x} \\ \dfrac{\partial u}{\partial {}_0y} + \dfrac{\partial v}{\partial {}_0x} + \dfrac{\partial {}^t u}{\partial {}_0x}\dfrac{\partial u}{\partial {}_0y} + \dfrac{\partial {}^t u}{\partial {}_0y}\dfrac{\partial u}{\partial {}_0x} + \dfrac{\partial {}^t v}{\partial {}_0x}\dfrac{\partial v}{\partial {}_0y} + \dfrac{\partial {}^t v}{\partial {}_0y}\dfrac{\partial v}{\partial {}_0x} \end{pmatrix} \tag{8} $$

and

$$ {}_0\boldsymbol{\eta} = \begin{pmatrix} {}_0\eta_x \\ {}_0\eta_{xy} \end{pmatrix} = \begin{Bmatrix} \dfrac{1}{2}\left[\left(\dfrac{\partial u}{\partial {}_0x}\right)^2 + \left(\dfrac{\partial v}{\partial {}_0x}\right)^2\right] \\ \dfrac{\partial u}{\partial {}_0x}\dfrac{\partial u}{\partial {}_0y} + \dfrac{\partial v}{\partial {}_0x}\dfrac{\partial v}{\partial {}_0y} \end{Bmatrix} \tag{9} $$

where u and v denote incremental displacements in the x- and y-directions, respectively.

The second Piola-Kirchhoff stress vector at time t is

$$ {}^t_0\mathbf{S} = \begin{pmatrix} {}^t_0\sigma_x \\ {}^t_0\tau_{xy} \end{pmatrix} \tag{10} $$

The incremental second Piola-Kirchhoff stresses are related to the incremental Green-Lagrange strains as

$$ {}_0\mathbf{S} = {}_0\mathbf{C}_0\boldsymbol{\varepsilon} \tag{11} $$

where

$$ {}_0\mathbf{C} = \begin{pmatrix} K_{ep} & 0 \\ 0 & k'G \end{pmatrix} \tag{12} $$

${}_0\mathbf{C}$ is the material property matrix for an isotropic material, while K_{ep} and G represent normal stress tangent modulus and shear modulus, respectively. Parameter k' is the shear shape factor which takes into account the nonuniform shear stress distribution across beam thickness.

Using the approximations ${}_0\mathbf{S} = {}_0\mathbf{C}_0\mathbf{e}$ and $\delta\boldsymbol{\varepsilon} = \delta\mathbf{e}$, (3) can now be linearized as

$$ \int_{{}_0V} {}_0\mathbf{e}^T {}_0\mathbf{C}\delta({}_0\mathbf{e})\, {}^0dV + \int_{{}_0V} {}^t_0\mathbf{S}^T\delta({}_0\boldsymbol{\eta})\, {}^0dV = {}^{t+\Delta t}\Pi - \int_{{}_0V} {}^t_0\mathbf{S}^T\delta({}_0\mathbf{e})\, {}^0dV \tag{13} $$

The governing finite-element equations can be developed using (13). The basic steps in the derivation of the governing finite-element equations are the same as those used in linear analysis: the selection of the interpolation functions and the interpolation of the element coordinates and displacements with these functions in the governing continuum mechanics equations.

The incremental displacement at time $t + \Delta t$ can be shown to be represented by

$$ u = {}^{t+\Delta t}x - {}^t x = \sum_{k=1}^{3} N_k u_k - \frac{sh}{2}\sum_{k=1}^{3} N_k(\cos {}^t\theta_k)\theta_k \tag{14a} $$

$$ v = {}^{t+\Delta t}y - {}^t y = \sum_{k=1}^{3} N_k v_k - \frac{sh}{2}\sum_{k=1}^{3} N_k(\sin {}^t\theta_k)\theta_k \tag{14b} $$

where k is the node number; and N_k are the interpolation functions as defined in Fig. 2. Other symbols are also defined in Fig. 2.

Using the above interpolation functions, (13) can be expressed as

$$ {}^t_0\mathbf{K}_N\mathbf{U} = ({}^t_0\mathbf{K}_L + {}^t_0\mathbf{K}_{NL})\mathbf{U} = {}^{t+\Delta t}\mathbf{R} - {}^{t+\Delta t}_0\mathbf{F} \tag{15} $$

where

$$ \mathbf{U} = (u_1, v_1, \theta_1, u_2, v_2, \theta_2, u_3, v_3, \theta_3)^T $$

$$ \delta(\mathbf{U}^T){}^t_0\mathbf{K}_L\mathbf{U} = \delta(\mathbf{U}^T)\left(\int_{{}_0V} {}^t_0\mathbf{B}_L^T {}_0\mathbf{C}^t_0\mathbf{B}_L\, {}^0dV\right)\mathbf{U} = \int_{{}_0V} {}_0\mathbf{e}^T {}_0\mathbf{C}\delta({}_0\mathbf{e})\, {}^0dV $$

$$ \delta(\mathbf{U}^T){}^t_0\mathbf{K}_{NL}\mathbf{U} = \delta(\mathbf{U}^T)\left(\int_{{}_0V} {}^t_0\mathbf{B}_{NL}^T {}^t_0\mathbf{S}^t_0\mathbf{B}_{NL}\, {}^0dV\right)\mathbf{U} = \int_{{}_0V} {}^t_0\mathbf{S}^T\delta({}_0\boldsymbol{\eta})\, {}^0dV $$

$$ \delta(\mathbf{U}^T){}^{t+\Delta t}_0\mathbf{F} = \delta(\mathbf{U}^T)\int_{{}_0V} {}^t_0\mathbf{B}_L^T {}^t_0\mathbf{S}\, {}^0dV = \int_{{}_0V} {}^t_0\mathbf{S}^T\delta({}_0\mathbf{e})\, {}^0dV \tag{16} $$

$\mathbf{B}_L$ and $\mathbf{B}_{NL}$ are the strain-displacement transformation matrices. The solution of (15) can be obtained by using an incremental-iterative technique such as the Newton-Raphson method, as will be discussed later.

To simulate the behavior of a nail subjected to reversed cyclic loading with acceptable accuracy and numerical efficiency, the model by Filippou et al. (1983) was adopted to represent the stress-strain relationship of the nail material.

The Filippou-Bertero-Popov model takes on the form

$$ \sigma^* = b\varepsilon^* + \frac{(1-b)\varepsilon^*}{(1+\varepsilon^{*R})^{1/R}} \tag{17} $$

where

$$ \varepsilon^* = \frac{\varepsilon - \varepsilon_r}{\varepsilon_0 - \varepsilon_r}; \quad \sigma^* = \frac{\sigma - \sigma_r}{\sigma_0 - \sigma_r} \tag{18a,b} $$

Eq. (17) represents a curved transition from a straight line asymptote with slope E_0 to another asymptote with slope E_1 [lines (a) and (b), respectively, in Fig. 3]. The parameters σ_0 and ε_0 are stress and strain at the point where the two asymptotes under consideration meet. Similarly, σ_r and ε_r are stress and strain at the point where the last strain reversal with stress of equal sign took place. The symbol b is the strain hardening ratio, which is E_1/E_0, and R is a parameter that influences the shape of the transition curve and is used to represent the Bauschinger effect [Sandor (1972)] and the low cycle fatigue characteristics. Parameter R takes the form

$$ R = R_0 - \frac{a_1\xi}{a_2 + \xi} \tag{19} $$

where ξ = absolute maximum strain difference, which is updated following a strain reversal; R_0 = value of R during first loading; and a_1, a_2 = experimentally determined parameters.

The model also accounts for strain hardening by shifting the position of the yield asymptote before computing the new

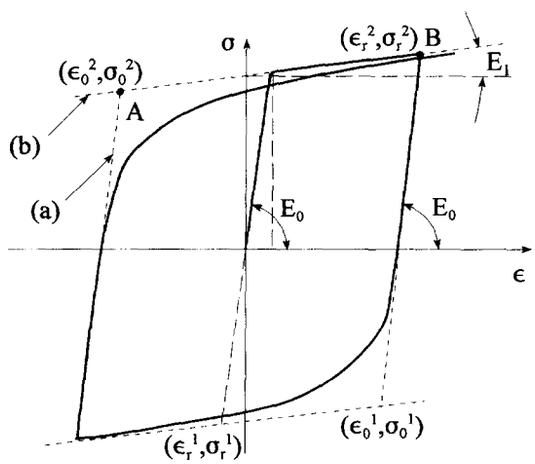

FIG. 3. Stress-Strain Model for Nail Material by Filippou et al. (1983)

asymptote intersection point following a strain reversal (Fig. 4). The imposed stress shift of the yield asymptotes is

$$\frac{\sigma_{st}}{\sigma_y} = a_3 \left(\frac{\epsilon_{max}}{\epsilon_y} - a_4 \right) \tag{20}$$

where σ_{st} = shift stress; ϵ_{max} = absolute maximum strains at the instant of strain reversal; σ_y, ϵ_y = yield stress and yield strain; and a_3, a_4 = experimentally determined parameters.

Wood Deformation

A two-node spring element is used to represent the embedment behavior of wood under loading by the fastener. Fig. 5 shows the element in the global and local coordinate systems. Based on equilibrium equations, the stiffness matrix of a spring element can be directly derived as follows,

$$\mathbf{K}_M = K_{em} \begin{pmatrix} 1 & -1 \\ -1 & 1 \end{pmatrix} \tag{21}$$

where K_{em} = tangential stiffness of the load-embedment relationship of wood.

A hysteresis model representing the load-embedment relationship of wood has been developed by Chui and Ni (1997) as part of the current study. The model consists of two parts: envelope curve and hysteresis loop, as shown in Fig. 6. For the envelope curve, Chui and Ni (1997) found that degradation in strength occurred under reversed cyclic loads. Therefore, the envelope curve is represented by the peak load P_p; initial stiffness, K_0; enforcing stiffness, K_1; and degrading stiffness, K_2 [Fig. 6(a)]. For the hysteresis loops, four equations were

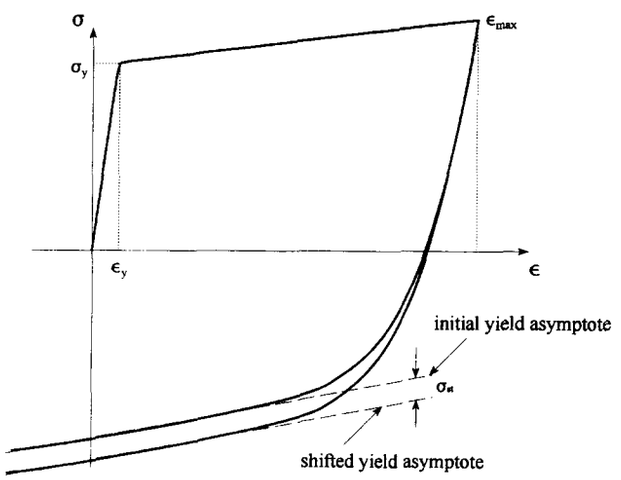

FIG. 4. Stress Shift Caused by Strain Hardening of Nail Material

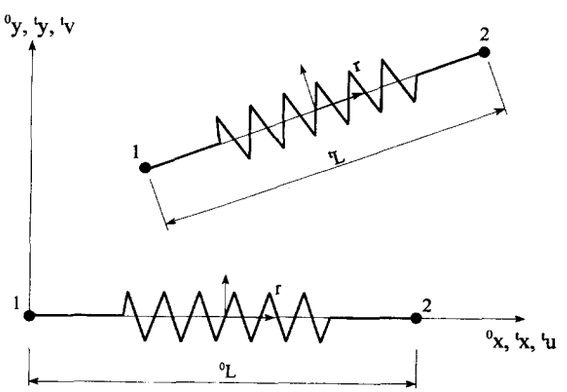

FIG. 5. Two-Node Spring Element Representing Embedment Behavior of Wood

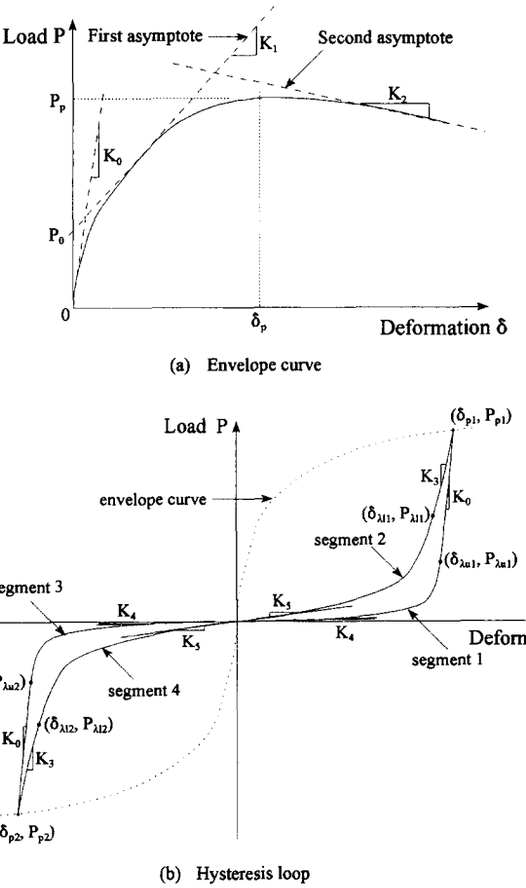

FIG. 6. Load-Embedment Model for Wood by Chui and Ni (1997)

used to define the loops under load reversal [Fig. 6(b)]. Each loop is completely defined by the stiffness parameters K_0, K_3, K_4, and K_5, and the coordinates of three of the points in each half loop. The equations representing envelope curve and different segments of the loops have been presented by Chui and Ni (1997) and are not repeated here.

The hystereis model described in Chui and Ni (1997) is adequate when the loading is regular and the amplitudes of the loading function are monotonically increasing. In practice, however, reversed cyclic loading conditions such as those arising from earthquakes or hurricanes are rarely regular in nature and are likely to be pseudorandom. Therefore, in order for the finite-element model to have any practical value, a set of so-called path rules must be developed. In this study, these rules were developed for nailed timber joints based on observations from tests conducted by the writers. In general, path rules are required if, during loading or unloading, the direction of loading reverses before reaching the envelope curve of the hysteresis loop. Rules for two situations are required. The first situation occurs when the load direction reverses during loading [Fig. 7(a)]. If the path BC continues its loading path, it will reach point A′ on the envelope curve. The unloading path after reaching point A′ would follow the dotted curve A′C′D. If, however, the direction of loading reverses when it reaches point C, the rule developed is that it will follow path CD, so that the displacement U_1 at any load level P_2 is related to curve A′C′D as shown by the equation in Fig. 7(a).

Another situation in which path rules are required is illustrated by path CDE in Fig. 7(b). It occurs when during unloading the load reverses direction at D before it reaches the zero slip location. The path follows DE. The developed path rule is that at any load level P_2, the slip U_1 is related to curve BD′C as is indicated in Fig. 7(b).

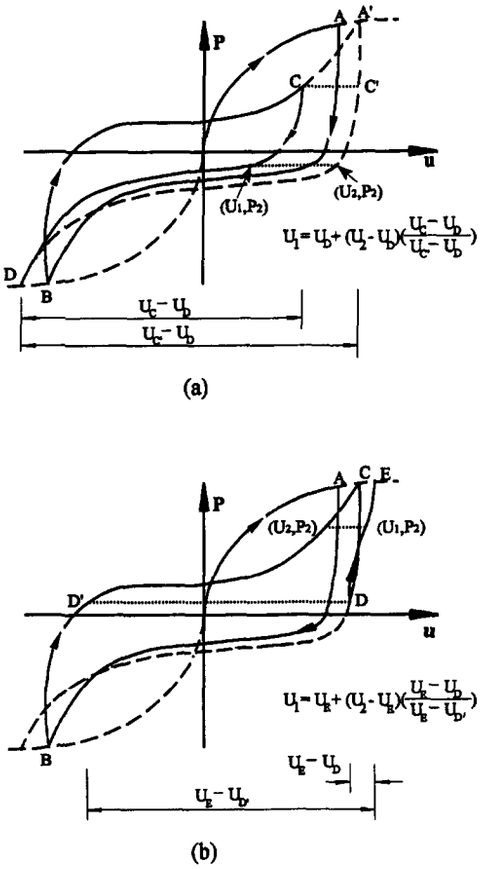

FIG. 7. Proposed Path Rules for Load-Embedment Response of Wood

Friction between Fastener Shank and Wood

A linkage element was introduced in the finite-element analysis to represent the friction between the fastener and wood. This approach was also used for modeling bond-slip relations in reinforced concrete structures [Bangash (1989)]. The element is similar to the type shown in Fig. 6. The stiffness matrix of the element is given as

$$\mathbf{K}_F = K_{ef}\begin{pmatrix} 1 & -1 \\ -1 & 1 \end{pmatrix} \tag{22}$$

where K_{ef} = tangent stiffness of the friction between fastener shank and wood.

In the friction model, a function $f(\delta_r)$ was introduced to take account of the friction developed under reversed cyclic loading, as shown in Fig. 8. The frictional force f_t is linked to the slippage between wood and fastener by the relationship

$$f_t = \mu f_n f(\delta_r) \tag{23}$$

where μ = friction coefficient; and f_n = normal pressure.

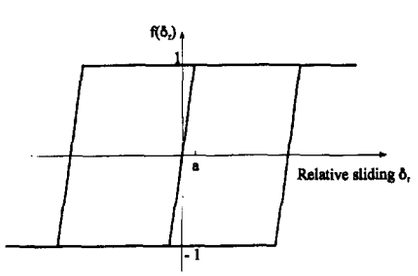

FIG. 8. Wood-Nail Friction Model

Incremental-Iterative Solution Technique

A common solution scheme for the type of nonlinear problem is the Newton-Raphson method [Oden (1972)]. Solutions are obtained from the following iteration scheme:

$$^{t+\Delta t}\mathbf{K}^{(i-1)}\mathbf{U}^{(i)} = {}^{t+\Delta t}\mathbf{R} - {}^{t+\Delta t}\mathbf{F}^{(i-1)} \tag{24}$$

The displacement increment correction $\mathbf{U}^{(i)}$ is used to obtain the next displacement approximation

$$^{t+\Delta t}\mathbf{U}^{(i)} = {}^{t+\Delta t}\mathbf{U}^{(i-1)} + \mathbf{U}^{(i)} \tag{25}$$

This incremental-iteration scheme is based on load control. Because, under extreme loading, the response of a structural component is displacement driven, it is therefore more appropriate to use an incremental displacement control scheme.

Considering the incremental displacement control, (24) can be rewritten as [Batoz and Dhatt (1979)]

$$^{t+\Delta t}\mathbf{K}^{(i-1)}\mathbf{U}^{(i)} = P^{(i)}\mathbf{\Phi} + {}^{t+\Delta t}\boldsymbol{\psi}^{(i-1)} \tag{26}$$

where Φ = reference externally applied nodal load vector; $P^{(i)}$ = incremental load parameter for iteration (i); and $^{t+\Delta t}\boldsymbol{\psi}^{(i-1)}$ = net out-of-balance force acting on the structure at the conclusion of iteration (i − 1), which is equal to $^{t+\Delta t}\mathbf{R}^{(i-1)} - {}^{t+\Delta t}\mathbf{F}^{(i-1)}$.

For proportional loading the external forces $^{t+\Delta t}\mathbf{R}^{(i-1)}$ at the conclusion of the previous iteration may be expressed as

$$^{t+\Delta t}\mathbf{R}^{(i-1)} = {}^{t+\Delta t}P^{(i-1)}\mathbf{\Phi} \tag{27}$$

Suppose that a solution at time t with displacement $^t\mathbf{U}$ and load parameter ^tP is obtained. At time $t + \Delta t$, instead of varying the load parameter, the qth component of $^t\mathbf{U}$ is incremented by U_q. The initial solution vector can be redefined as

$$^{t+\Delta t}\mathbf{U}^{(0)} = {}^t\mathbf{U}; \quad {}^{t+\Delta t}U_q^{(0)} = {}^tU_q + U_q \tag{28a,b}$$

To obtain $^{t+\Delta t}\mathbf{U}^{(i)}$ and $^{t+\Delta t}P^{(i)}$ with $^{t+\Delta t}U_q$ fixed, the solution of (26) can be obtained by first calculating $U_a^{(i)}$ and $U_b^{(i)}$ as

$$^{t+\Delta t}\mathbf{K}^{(i-1)}\mathbf{U}_a^{(i)} = {}^{t+\Delta t}\boldsymbol{\psi}^{(i-1)}; \quad {}^{t+\Delta t}\mathbf{K}^{(i-1)}\mathbf{U}_b^{(i)} = \mathbf{\Phi} \tag{29a,b}$$

and obtaining the incremental load parameter $P^{(i)}$ from the following constraint equation:

$$U_q^{a(i)} + P^{(i)}U_q^{b(i)} = U_q^{(i)} = 0 \tag{30}$$

Then the incremental displacement change for this iteration is

$$\mathbf{U}^{(i)} = \mathbf{U}_a^{(i)} + P^{(i)}\mathbf{U}_b^{(i)} \tag{31}$$

The total displacement and load levels are then updated from the previous iteration by

$$^{t+\Delta t}\mathbf{U}^{(i)} = {}^{t+\Delta t}\mathbf{U}^{(i-1)} + \mathbf{U}^{(i)}; \quad {}^{t+\Delta t}P^{(i)} = {}^{t+\Delta t}P^{(i-1)} + P^{(i)} \tag{32a,b}$$

Using an incremental displacement control, (2) can be rewritten as

$$^{t+\Delta t}\begin{bmatrix} \mathbf{K}_N + \mathbf{K}_{LM} + \mathbf{K}_{LF} + \mathbf{K}_{UM} + \mathbf{K}_{UF} & -\mathbf{K}_{LM}\mathbf{I} \\ -(\mathbf{K}_{LM}\mathbf{I})^T & \sum_{i=1}^{N_L}\mathbf{K}_{LM_i} \end{bmatrix}^{(i-1)} \begin{pmatrix} \mathbf{U}_N \\ U_q \end{pmatrix}^{(i)}$$

$$= P^{(i)}\begin{pmatrix} 0 \\ 1 \end{pmatrix} + {}^{t+\Delta t}\begin{pmatrix} \mathbf{R} - \mathbf{F} \\ P - f \end{pmatrix}^{(i-1)} \tag{33}$$

Eq. (33) is in the form to which the above displacement control solution technique can be readily applied.

VALIDATION OF MODEL

Single-nailed joint tests were conducted for verification purposes. Three joint types made with different combinations of wood type and nail size were tested: maple-to-maple with a no. 9 gauge common nail, spruce-to-spruce with a no. 9 gauge

common nail, and plywood-to-spruce with a no. 11 1/2 gauge common nail. The nominal nail dimensions were: 2.86 mm × 57 mm for the no. 11 1/2 gauge and 3.76 mm × 78 mm for the no. 9 gauge. The joints were subjected to a sawtooth displacement controlled loading function with increasing displacement peaks. A loading rate of 0.25 Hz was used. The peak increment was 0.1 mm before a displacement of 1 mm; then the increment was increased to 0.2 mm until failure or a large displacement of 10 mm was reached in one direction.

In addition to the joint tests, tests were also conducted to obtain stress-strain characteristics of the nail and load-embedment relationship of the wood under reversed cyclic loading. For nail material, ASTM F680-80 [*Standard* (1990)] recommends that steel wire used to make the nails should be tested for characterization of material properties. Reversed cyclic loading tests were conducted on specimens cut from steel wire to extract the parameters of the Filippou-Bertero-Popov model. In this study, coiled steel wires used to make the gauge no. 11 1/2 and gauge no. 9 common nails were ordered from the nail manufacturer. The mean diameters of the coiled wires were measured as 2.79 mm and 3.69 mm, respectively. Five replicates were used for each size. Table 1 shows the mean and standard deviation of the identified parameters of the stress-strain model of the nail. In general, it can be seen that the modulus values for the two nails are similar, but the yield strength of the smaller nail is higher. Also, the hysteresis loops for the smaller nail appeared to be narrower than those of the larger nail, indicating a lower capacity for energy absorption.

To obtain the load-embedment properties of the wood used in the validation joint tests, embedment tests were conducted using a specially designed apparatus. The following nail-wood combinations were tested: no. 9 gauge nail-spruce; no. 9 gauge nail-maple; no. 11 1/2 gauge nail-spruce and no. 11 1/2 gauge nail-plywood. Ten replicates were used for each combination. The loading rate and function were similar to those used in the joint tests. The parameters of the hysteresis model were then extracted from the test data using a least-squares method. Further details on test procedure and test results are reported in Chui and Ni (1997) for the four combinations of nail size and wood type.

In order to ensure that the embedment specimens were matched to those for the verification joint tests, material for joint and corresponding embedment tests was cut from the same block. The wood material and the joints were stored in a controlled environment of 20 ± 3°C temperature and 65 ± 2% relative humidity prior to testing.

In the finite-element analysis, 20 elements were used for the point-side member. 20 elements were used for the head-side member of the spruce-to-spruce and maple-to-maple joints, and 10 elements for the plywood-to-spruce nailed joint. The friction coefficient μ between nail and wood was taken to be

TABLE 1. Mean and Standard Deviation of Identified Parameters for Filippou-Bertero-Popov Model for Nail Material

Model parameter (1)	Gauge No. 11 1/2 Common Nail		Gauge No. 9 Common Nail	
	Mean (2)	Standard deviation (3)	Mean (4)	Standard deviation (5)
R_0	3.82	0.14	2.98	0.09
b	0.0015	0.0001	0.0010	0.0002
E_0 (N/mm^2)	193,957	8,484	192,662	3,368
σ_y (N/mm^2)	810	7	690	7
ε_y (mm/mm)	0.0042	0.0002	0.0036	0.0001
a_1	0.850	0.056	0.0049	0.0003
a_2	0.151	0.001	0.149	0.002
a_3	0.0079	0.0003	−0.0149	0.0005
a_4	0.201	0.002	0.200	0.003

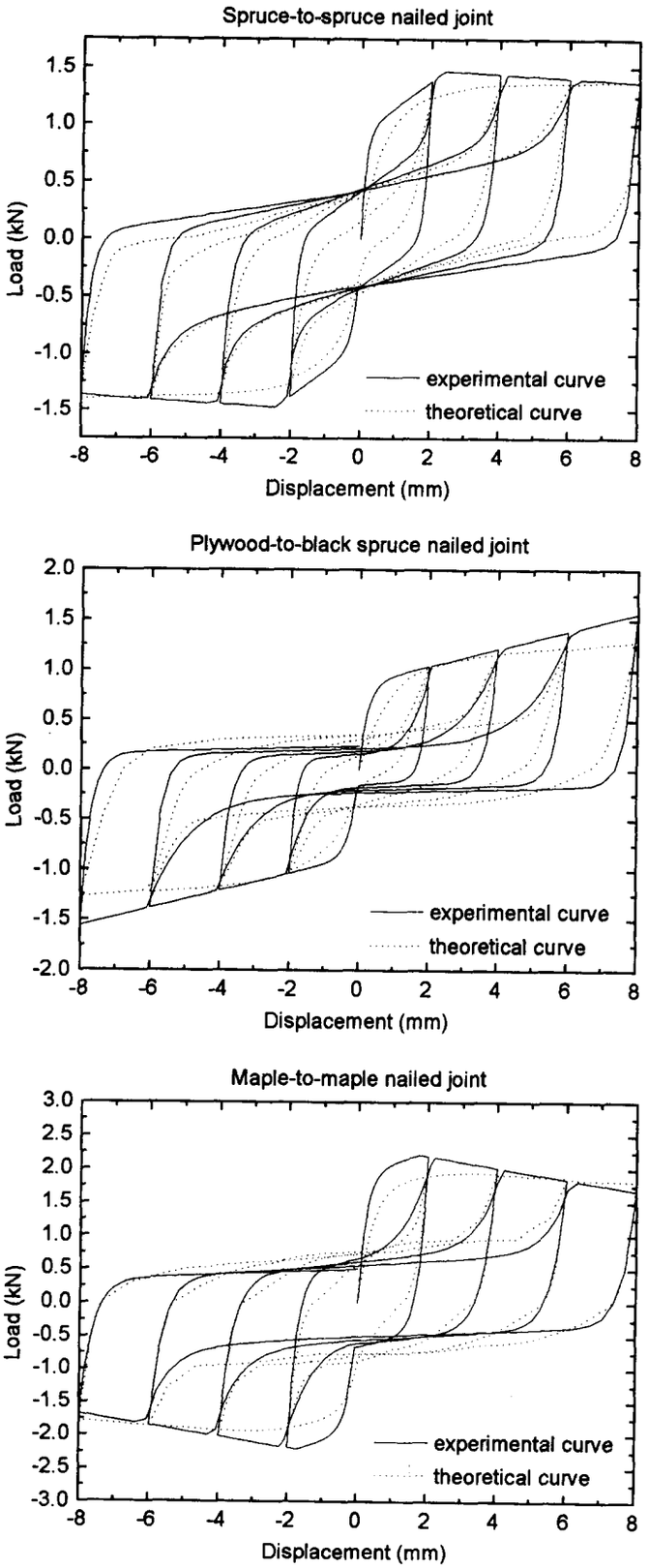

FIG. 9. Comparison of Predicted and Experimental Hysteresis Loops

0.1 following the test data obtained by Erki (1990). The analysis was carried out under joint slip displacement, starting from zero displacement until the joint displacement reached a value of 8 mm.

Fig. 9 shows for each joint type a comparison of the model

prediction with experimental data. In each case four complete cycles were calculated with peak displacement at 2 mm, 4 mm, 6 mm, and 8 mm, respectively. Fig. 9 shows that the predicted hysteresis response is generally in good agreement with the experimental results. Two areas of discrepancy can be noted. The first relates to the underestimation of load for a given displacement level of the evelope curve. This is thought to be caused by the fact that the model uses discrete springs to represent the embedment properties of wood. These springs are assumed to act independently of each other. This approach leads to a less stiff system since, in reality, these springs are not independent of each other. The second factor relates to the relatively large discrepancy between predicted and test curves at small displacement levels. This is caused by the fact that the proposed hysteresis model provides a better fit at larger displacements because it is intended for a pinched hysteresis loop. At small displacements, pinching of the hysteresis loop is not evident.

CONCLUSION

This paper describes the development and validation of a nonlinear finite-element model for predicting load-slip response of a single nailed joint under a reversed cyclic lateral load. The results show the finite-element model predicts the hysteresis behavior of nailed joints with good accuracy. The availability of this model will enable the determination of nailed joint characteristics such as strength degradation, energy absorption and ductility from material properties without the need to conduct tests on joint assemblies. These joint characteristics are important indicators of performance of timber structures containing nailed joints under extreme loading conditions, and as such have a large bearing on the design of a structure containing such joints. For example, the model can be used to determine the ductility ratio and hence the design force of a joint. With minor modifications, the model can be used to analyze the load-displacement response of joints containing other dowel-type fasteners, such as bolts, as long as the joint failure is due to the yielding of the fastener.

ACKNOWLEDGMENTS

The writers wish to thank the Canadian Wood Council, Ottawa, and the Natural Sciences and Engineering Research Council of Canada, Ottawa, for providing the funding for this study.

APPENDIX I. REFERENCES

Bangash, M. Y. H. (1989). *Concrete and concrete structures: numerical modelling and application.* Elsevier Science Publishing Co. Inc., New York, N.Y.

Bathe, K. J. (1982). *Finite element procedures in engineering analysis.* Prentice-Hall, Inc., Englewood Cliffs, N.J.

Batoz, J. L., and Dhatt, G. (1979). "Incremental displacement algorithms for non-linear problems." *Int. J. Numer. Methods in Engrg.*, 14, 1262–1267.

Ceccotti, A., and Vignoli, A. (1990). "Engineered timber structures: an evaluation of their seismic behaviour." *Proc., 1990 Int. Timber Engrg. Conf.*, Science University of Tokyo, Tokyo, Japan, 946–953.

Ceccotti, A., Vignoli, A., and Giordana, S. (1994). "Seismic tests on full-scale timber structures." *Proc., Pacific Timber Engrg. Conf.*, Vol. 1, Timber Research and Development Advisory Council, Fortitude Valley MAC, Queensland, Australia, 232–240.

Chui, Y. H., and Ni, C. (1997). "Load-embedment response of timber to reversed cyclic load." *Wood and Fiber Sci.*, 29(2), 148–160.

Cruz, H. M. P. (1993). "Nailed timber joints subjected to alternating load cycles," PhD thesis, University of Brighton, Brighton, U.K.

Daneff, G., Smith, I., and Chui, Y. H. (1996). "Test protocol for evaluating seismic behaviour of connections." *Proc., Int. Wood Engrg. Conf.*, Vol. 1, Louisiana State University, Baton Rouge, La, 37–44.

Dolan, J. D. (1989). "The dynamic response of timber shear walls," PhD thesis, University of British Columbia, Vancouver, B.C., Canada.

Dolan, J. D., and Madsen, B. (1992). "Monotonic and cyclic nail connection tests." *Can. J. Civ. Engrg.*, 19(1), 97–104.

Erki, M. A. (1990). "Modelling the load-slip behaviour of timber joints with mechanical fasteners." PhD thesis, University of Toronto, Toronto, Ont., Canada.

Filippou, F. C., Bertero, V. V., and Popov, E. P. (1983). Effects of bound deterioration on hysteretic behaviour of reinforced concrete joints." *EERC Rep. No. 83-19*, University of California, Berkeley, Calif.

Foliente, G. (1994). "Hysteresis characterization and modelling of timber joints and structures." *Proc., Pacific Timber Engrg. Conf.*, Vol. 2, Timber Research and Development Advisory Council, Fortitude Valley MAC, Queensland, Australia, 26–35.

Foschi, R. O. (1974). "Load-slip characteristics of nails." *Wood Sci.*, 7(1), 69–74.

Gutshall, S. T., Dolan, J. D., and McLain, T. M. (1994). "Monotonic and cyclic short-term performance of nailed and bolted timber connections." *Rep. No. TE-1994-005*, Dept. of Wood Sci. and Forest Products, Virginia Polytechnic Institute and State University, Blacksburg, Va.

Hattar, C. P., and Cheng, J. J. R. (1995). "Development of moment connections in glued-laminated Alberta spruce and pine timber." *Res. Rep.*, Dept. of Civ. Engrg., University of Alberta, Edmonton, Alta., Canada.

Kivell, B. T., Moss, P. J., and Carr, A. J. (1981). "Hysterestic modelling of moment resisting nailed timber joints." *Bull. of New Zealand Nat. Soc. for Earthquake Engrg.*, 14(4), 233–243.

Ni, C., and Chui, Y. H. (1994). "Response of nailed wood joints to dynamic loads." *Proc., Pacific Timber Engrg. Conf.*, Vol. 2, Timber Research and Development Advisory Council, Fortitude Valley MAC, Queensland, Australia, 9–18.

Ni, C., Smith, I., and Chui, Y. H. (1993). "A simplified approach for predicting response of nailed wood joints to reversed cyclic loads." *Proc., Annu. Conf.*, Vol. 2, Canadian Society for Civil Engineering, Montreal, Que., Canada, 375–484.

Oden, J. T. (1972). *Finite elements of nonlinear continua.* McGraw-Hill Book Co., Inc., New York, N.Y.

Paulay, T., and Priestley, M. J. N. (1992). *Seismic design of reinforced concrete and masonry buildings.* John Wiley & Sons, Inc., New York, N.Y.

Prion, H., and Foschi, R. O. (1994). "Cyclic behaviour of dowel type connections." *Proc., Pacific Timber Engrg. Conf.*, Vol. 2, Timber Research and Development Advisory Council, Fortitude Valley MAC, Queensland, Australia, 19–25.

Sandor, B. I. (1972). *Fundamentals of cyclic stress and strain.* The University of Wisconsin Press, Madison, Wis.

Soltis, L. A., and Mtenga, P. V. A. (1985). "Strength of nailed wood joints subjected to dynamic load." *Forest Products J.*, 35(11/12), 14–18.

Standard test methods for nails; F680-80. (1990). ASTM, Philadelphia, Pa.

Stewart, W. G. (1987). "The seismic design of plywood sheathed shear walls," PhD thesis, University of Canterbury, Christchurch, New Zealand.

APPENDIX II. NOTATION

The following symbols are used in this paper:

a_1, a_2, a_3, a_4 = parameters of Filippou-Bertero-Popov model for fastener;

$\mathbf{B}_L$, $\mathbf{B}_{NL}$ = strain-displacement transform matrices;

b = parameter of Filippou-Bertero-Popov model for fastener;

$\mathbf{C}$ = material property matrix for fastener material;

E_0, E_1 = stiffness parameters of Filippou-Bertero-Popov model for fastener;

$\mathbf{F}$ = vector of fastener internal point forces;

f = total embedment force of point-side member;

f_n = normal pressure applied by fastener on wood;

f_t = frictional force developed between fastener on wood;

$f(\delta_r)$ = friction function between fastener and wood;

G = shear modulus of fastener;

h = height of beam element;

$\mathbf{I}$ = unit vector;

K_{ef} = tangent stiffness of friction between fastener and wood;

K_{em} = tangential stiffness of wood foundation;
K_{ep} = normal stress tangent modulus of fastener;
$\mathbf{K}_F$ = stiffness matrix of a friction element between fastener and wood;
$\mathbf{K}_L$ = linear part of stiffness matrix of fastener;
$\mathbf{K}_{LF}$ = friction stiffness matrix of point-side member;
$\mathbf{K}_{LM}$ = embedment stiffness matrix of point-side member;
$\mathbf{K}_M$ = stiffness matrix of wood foundation;
$\mathbf{K}_N$ = stiffness matrix of fastener;
$\mathbf{K}_{NL}$ = nonlinear part of stiffness matrix of fastener;
$\mathbf{K}_{UF}$ = friction stiffness matrix of head-side member;
$\mathbf{K}_{UM}$ = embedment stiffness matrix of head-side member;
k' = shear shape factor of fastener;
N_1, N_2, N_3 = interpolation functions;
P = total applied load;
$\mathbf{R}$ = vector of externally applied nodal loads;
R, R_0 = parameters of Filippou-Bertero-Popov model for fastener;
r = local beam coordinate parallel to the beam axis;
$\mathbf{S}$ = second Piola-Kirchhoff stress vector;
s = local beam coordinate perpendicular to the beam axis;
$\mathbf{U}_N$ = deformation vector of fastener;
U_q = movement of point-side member;
u = fastener displacement in x-coordinate;
v = fastener displacement in y-coordinate;
γ_{xy} = beam shear strain;
$\boldsymbol{\varepsilon}$ = Green-Lagrange strain vector;
$\varepsilon^*, \varepsilon_0, \varepsilon_r, \varepsilon_y, \varepsilon_{max}$ = strain parameters of Filippou-Bertero-Popov model for fastener;
ε_x = beam axial strain in x-direction;
θ = fastener rotation;
μ = friction coefficient between fastener and wood;
ξ = parameter of Filippou-Bertero-Popov model for fastener;
Π = external virtual work in configuration at time $t + \Delta t$;
$\sigma^*, \sigma_0, \sigma_r, \sigma_{st}, \sigma_y$ = stress parameters of Filippou-Bertero-Popov model for fastener;
σ_x = beam axial stress in x-direction;
τ_{xy} = beam shear stress;
$\boldsymbol{\Phi}$ = vector of referenced externally applied nodal loads; and
$\boldsymbol{\psi}$ = vector of net out-of-balance forces.